Frequency Sensitivity Analysis of Coil-IDE Resonance Topology Circuit and Its Humidity Sensor Applications

Dong Liu, *Member, IEEE*, Qiao Chen, Haoran Li, Guiyun Tian, *Senior Member, IEEE*, Bin Gao, *Senior Member, IEEE*, Zhuhong Xiong, and Minqiang Li

***Abstract*—In this article, the frequency sensitivity of the Coil-interdigital electrode (IDE) sensor in different integrated topologies is studied. In particular, the expression of the resonance frequency of the Coil-IDE sensor both in series and parallel topological structure is derived. The sensitivity of frequency to IDE capacitance was analyzed, and two new results can be found 1) due to the existence of coil winding capacitance and grounding capacitance, the Coil-IDE topology circuit has been changed, which causes the Coil-IDE parallel topology structure has a higher frequency sensitivity than series and 2) not only the topology structure but also the parameters such as coil inductance and IDE capacitance have the regulatory effect on the frequency sensitivity. After analysis, an experiment of a Coil-IDE humidity sensor was applied to verify the presented results. The parallel frequency of the Coil-IDE parallel structure having a higher sensitivity was confirmed. The error of the proposed formula predicting the regulatory effect of parameters on frequency sensitivity was discussed. The error is as low as 7.57%, which shows the beneficial aspect of the integrated design of Coil-IDE sensor both in topological structure and parameters.**

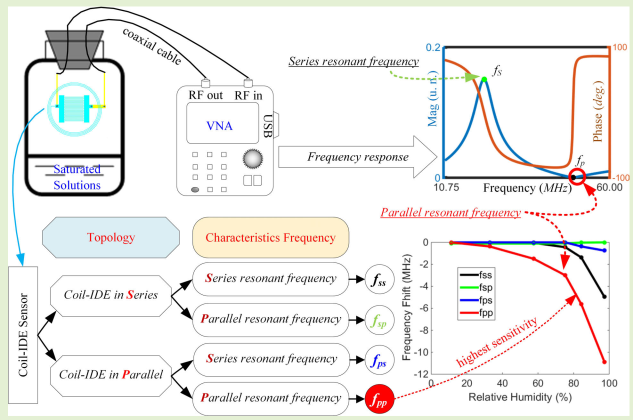

***Index Terms*—Frequency sensitivity, humidity, inductance–capacitance (*LC*), parallel resonance frequency.**

I. Introduction

INDUCTIVE-CAPACITIVE resonant sensor has also been widely researched in the field of humidity sensing. Feng et al. [1] produced a polyethylene terephthalate (PET)-based *LC* humidity sensor with a working frequency of 157 MHz. The sensor has a sensitivity of 1804 ppm/%RH in the humidity, with a range of 20%–90%. Dong et al. [2] designed 30 MHz *LC* passive wireless sensors using graphene oxide as humidity-sensitive materials, and these sensors show a humidity sensitivity of 1244 ppm/%RH within the humidity range of 15%–90%. Martuza et al. [3] proposed a 160 MHz *LC* flexible passive wireless sensor and obtained a humidity sensitivity of 562 ppm/%RH within the humidity range of 30%–90%. Deng et al. [4] reported a 140 MHz *LC* wireless humidity sensor fabricated on flexible PET substrates and got a high humidity sensitivity of 1000 ppm/%RH within the humidity range of 20%–95%. Xie et al. [5] provided a 55 MHz inductor–capacitor (*LC*) passive wireless humidity sensor and achieved a high humidity sensitivity of 1161 ppm/%RH within the humidity range of 15%–90%. Su et al. [6] applied a 170 MHz *LC* wireless passive humidity sensor based on MoS2 nanoflakes and obtained a high humidity sensitivity of 447 ppm/%RH within the humidity range of 10%–95%. Compared with other humidity sensors such as quartz crystal microbalance (QCM) [7], interdigital electrodes-piezoelectric quartz crystal (IDE-PQC) [8], or surface acoustic wave (SAW) [9], the inductive-capacitive resonant sensor has some

Manuscript received 22 February 2023; revised 16 March 2023; accepted 20 March 2023. Date of publication 28 March 2023; date of current version 1 May 2023. The work was supported in part by the National Natural Science Foundation of China under Grant 61971093, Grant 61527803, and Grant 61960206010; in part by the Department of Science and Technology of Sichuan Province under Grant 2019JDZH0020; and in part by the Key Laboratory of Nondestructive Testing of Fujian Polytechnic Normal University under Grant S2-KF2013. The associate editor coordinating the review of this article and approving it for publication was Dr. Hui Jiang. *(Corresponding author: Bin Gao.)*

Dong Liu, Qiao Chen, Haoran Li, and Bin Gao are with the School of Automation Engineering, University of Electronic Science and Technology of China, Chengdu, Sichuan 611731, China (e-mail: dong.liu@uestc.edu.cn; qiaochen@std.uestc.edu.cn; horn_lee@std.uestc.edu.cn; bin_gao@uestc.edu.cn).

Guiyun Tian is with the School of Engineering, Newcastle University, NE1 7RU Newcastle upon Tyne, U.K. (e-mail: g.y.tian@ncl.ac.uk).

Zhuhong Xiong is with Sichuan Institute of Building Research Company Ltd., Chengdu 610081, China (e-mail: 28511667@qq.com).

Minqiang Li is with the College of Materials Science and Engineering, Sichuan University, Chengdu, Sichuan 610054, China (e-mail: 1816453911@qq.com).

Digital Object Identifier 10.1109/JSEN.2023.3260967

disadvantages as response time and etc.; however, it has some advantages [10] in high sensitivity, easy integration, and low cost. Furthermore, as the progress of micro/nanofabrication technologies, the advantages of easy integration and low cost are becoming more obvious [5], [11], [12]. Therefore, it is widely applied in industry [1], agriculture [13], smart homes [14], food safety, and human health monitoring [15].

Among those capacitive sensors, IDE capacitive sensor has received attention due to its coplanarity, convenience in manufacturing, and capacity controllability. Chen et al. [16] pointed out the influence of capacitance parameters on the frequency sensitivity of the IDE capacitive sensor. Biswas et al. [13] proposed a method to trim the electric field shape through the structure of the IDE. Then, the sensitivity of the IDE capacitive sensor to the soil moisture can be enhanced through the edge field effect.

As an integrated network of inductors and capacitors, many integrated structures of the topological circuit have been adopted in inductive-capacitive resonant sensors. It includes *LC* in parallel [3], [17], *LC* in series [18], or a complex combination of series and parallel [19]. The influence of different schemes of the integrated inductive-capacitive resonant sensor on frequency sensitivity needs to be analyzed.

The inductive-capacitive resonant sensor, has the lowest impedance at the series resonance frequency and is easy to be extracted by the oscillator [20], [21], vector network analyzer (VNA) [4], [22], [23] or impedance analyzer [3]. Therefore, the series resonance frequency is widely used as the characteristic signal by colleagues and named as the resonance frequency.

In this article, the frequency sensitivity of the Coil-IDE integrated sensor is analyzed from two aspects of topological structure and characteristic frequency. We would like to draw the attention of colleagues to the characteristic frequencies beyond the series resonance frequency of the Coil-IDE integrated sensor. Both theoretical calculation and experiment show that the parallel resonance frequency of Coil-IDE has a higher sensitivity than the series resonance frequency, which is generally considered as the resonance frequency. This is due to the topological circuit change caused by the unavoidable existence of lead capacitance and grounding capacitance.

We first analyze the evolution of the topological circuits of inductive-capacitive resonant sensor, which considers the winding capacitance of inductors and instrument grounding capacitance. Second, the expressions of the resonance frequencies both in *LC* parallel and *LC* series topologies are given through the proposed inverse transform between the inductive-capacitive resonant sensor and the Butterworth-Van Dyke (BVD) model [24] of a piezoelectric crystal. Therefore, the frequency sensitivity can be compared according to the proposed formulas. Third, an inductive-capacitive resonant humidity sensor integrating coil inductor and IDE capacitor is given, and experimental data based on the regulatory effect of humidity on capacitance is obtained. Finally, the regulatory effect of the frequency sensitivity both on the circuit's topological structure and the electronic parameters of the sensor will be discussed. Thus, the proposed formula will be supported by the experimental data.

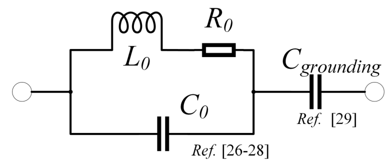

Fig. 1. Coil-IDE resonant topological circuits considering winding, coaxial, and grounding capacitance.

The article is organized as follows. Section II introduces the proposed theory of architecture and derivation. Section III respectively presents the analysis and a series of verifications and results. Finally, Section IV summarizes the findings of the work and concludes the article.

II. Methodology

We would like to analyze the frequency sensitivity of the Coil-IDE integrated sensor in two aspects: characteristic frequency selection and topological structure.

For the characteristic frequency selection, the modification of the characteristic frequency expression due to the existence of the unavoidable existence of lead capacitance and grounding capacitance has been derived, including the series resonance frequency [25] and the parallel resonance frequency [24]. Through the expression, the sensitivity can be analyzed mathematically and used as the theoretical criterion for characteristic frequency selection.

For the topological structure, the influence of the Coil-IDE topological structure on sensitivity has been analyzed, including Coil-IDE in series and parallel topological structure, respectively. Two topological structures and two characteristic frequencies combine into four frequencies. They are the series resonance frequency of the Coil-IDE series topological circuit (f_{ss}), the parallel resonance frequency of the Coil-IDE series topological circuit (f_{sp}), the series resonance frequency of the Coil-IDE parallel topological circuit (f_{ps}), and the parallel resonance frequency of the Coil-IDE parallel topological circuit (f_{pp}). By comparing the expression of the four frequencies, both effects of the characteristic frequency selection and topological structure on sensitivity will be analyzed.

A. Modification of the Characteristic Frequency Expression Due to the Topology Change Caused by Distribution Capacitance

Considering winding capacitance [26], [27], coaxial cable capacitance [28], and grounding capacitance [29], the topology of the Coil-IDE sensor is shown in Fig. 1.

Our previous work [19] has proved that the topological circuits in Fig. 1 are equivalent to the general electronic topology of quartz crystal (BVD model) shown in Fig. 2.

Furthermore, The equivalent conversion relationship from Figs. 1 to 2 is given as follows [19]:

$$\begin{cases} C_g = C + C_0' \\ C_0 = C_0'\left(1 + C_0'/C\right) \\ R_1 = RC^2/\left(C + C_0'\right)^2 \\ L_1 = LC^2/\left(C + C_0'\right)^2. \end{cases} \tag{1}$$

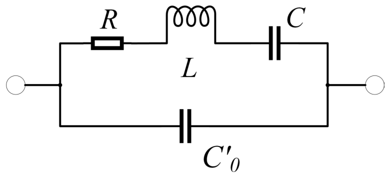

Fig. 2. General electronic topology of quartz crystal (BVD model).

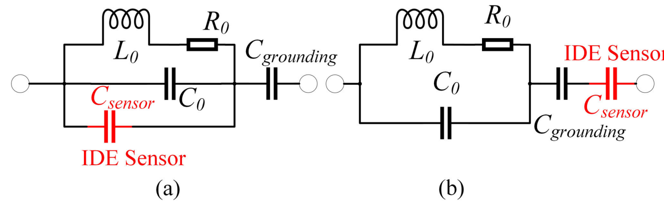

Fig. 3. Electronic topology of Coil-IDE sensor in different topological structures in: (a) parallel and (b) series.

So, the inverse conversion of the above equivalent conversion is not given. In this article, the inverse conversion is proposed, and it can be shown as follows:

$$\begin{cases} R = R_1\left(1 + C_0/C_g\right)^2 \\ L = L_1\left(1 + C_0/C_g\right)^2 \\ C = C_g^2/\left(C_g + C_0\right) \\ C_0' = \left(C_g C_0\right)/\left(C_g + C_0\right). \end{cases} \tag{2}$$

The series resonance frequency (f_s') in Fig. 2 is defined [24], [30] as the low-impedance of the resonance frequency and can be expressed as

$$f_s' = \frac{1}{2\pi}\sqrt{\frac{1}{LC}}. \tag{3}$$

The parallel resonance frequency (f_p') in Fig. 2 is defined [24] as the high-impedance of the resonance frequency and can be expressed as

$$f_p' = \frac{1}{2\pi}\sqrt{\frac{1}{LC} + \frac{1}{LC_0'}}. \tag{4}$$

Because topological circuits in Fig. 1 and topological circuits in Fig. 2 are equivalent, they will have the same frequency response curve and the same characteristic frequency, but the characteristic frequency will be expressed by different parameters.

Therefore, bring (2) into (3), and get the series resonance frequency (f_s) of the topological circuits in Fig. 1 as

$$f_s = \frac{1}{2\pi}\sqrt{\frac{1}{L_1\left(C_g + C_0\right)}}. \tag{5}$$

Bring (2) into (4), and get the parallel resonance frequency (f_p) of the topological circuits in Fig. 1 as

$$f_p = \frac{1}{2\pi}\sqrt{\frac{1}{L_1 C_0}}. \tag{6}$$

Comparing (3)–(6), it can be found that the frequency defined by $1/2\pi\sqrt{LC}$ represents the series resonant frequency for piezoelectric crystal in Fig. 2 but represents the parallel resonant frequency for the Coil-IDE sensor in Fig. 1.

The series resonant frequency is easy to be extracted from the resonant circuit, which is considered by most colleagues as the resonance frequency. The above derivation indicates that the resonant frequency (the series resonant frequency) cannot be described by $1/2\pi\sqrt{LC}$ in the Coil-IDE resonator. Instead, another characteristic frequency (the parallel resonance frequency) can be described by $1/2\pi\sqrt{LC}$.

For f_p, the total capacitance is $C_{\text{total}} = C_0$. For f_s, the total capacitance is $C_{\text{total}} = C_g + C_0$. By comparing form (6) to (5), it can be found that the variation rate of total capacitance caused by the variation of C_0 is bigger in (6) than in (5). In other words, the parallel resonance frequency will be more sensitive to the variation of the capacitance C_0.

B. Expression of Characteristic Frequency Under Different Topological Structures and Its Frequency Sensitivity Analysis

Next, consider the impact of the topological structure of the Coil-IDE sensor on sensitivity. Two topological structures are considered. They are Coil-IDE in series and Coil-IDE in parallel, respectively, shown in Fig. 3. In Fig. 3, The capacitance effect of the IDE sensor is simplified as a capacitor at the high frequency [16].

In Fig. 3(a), the series resonance frequency of the Coil-IDE series topology circuit (f_{ss}) should be

$$f_{\text{ss}} = \frac{1}{2\pi}\sqrt{\frac{1}{L_1\left(\frac{C_s C_g}{C_s + C_g} + C_0\right)}}. \tag{7}$$

The parallel resonance frequency of the Coil-IDE series topology circuit (f_{sp}) should be

$$f_{\text{sp}} = \frac{1}{2\pi}\sqrt{\frac{1}{L_1 C_0}}. \tag{8}$$

In Fig. 3(b), the series resonance frequency of the Coil-IDE parallel topology circuit (f_{ps}) should be

$$f_{\text{ps}} = \frac{1}{2\pi}\sqrt{\frac{1}{L_1\left(C_g + C_0 + C_s\right)}}. \tag{9}$$

The parallel resonance frequency of the Coil-IDE parallel topology circuit (f_{pp}) should be

$$f_{\text{pp}} = \frac{1}{2\pi}\sqrt{\frac{1}{L_1\left(C_0 + C_s\right)}}. \tag{10}$$

The sensitivity of frequencies to the capacitance of the IDE sensor can be judged by the derivative of the frequencies to C_s.

The derivatives of the four frequencies to the C_s are

$$\frac{df_{ss}}{dC_s} = \frac{-1}{4\pi}\sqrt{\frac{1}{L_1}}\left(\frac{C_s C_g}{C_s+C_g}+C_0\right)^{\frac{-3}{2}}\frac{C_g^2}{(C_s+C_g)^2} \tag{11}$$

$$\frac{df_{\text{sp}}}{dC_s} = 0 \tag{12}$$

$$\frac{df_{\text{ps}}}{dC_s} = \frac{-1}{4\pi}\sqrt{\frac{1}{L_1}}\left(C_g+C_0+C_s\right)^{\frac{-3}{2}} \tag{13}$$

$$\frac{df_{\text{pp}}}{dC_s} = \frac{-1}{4\pi}\sqrt{\frac{1}{L_1}}\left(C_0+C_s\right)^{\frac{-3}{2}}. \tag{14}$$

Formula (12) indicates that f_{sp} is not sensitive to C_s. Therefore, (11), (13), and (14) need to be compared.

First, compare (13) with (14). Because of existence of $(C_g+C_0+C_s) > (C_0+C_s)$, we can get

$$\text{abs}\left(\frac{df_{\text{ps}}}{dC_s}\right) < \text{abs}\left(\frac{df_{\text{pp}}}{dC_s}\right). \tag{15}$$

Second, compare (11) with (14). It is difficult to compare the two formulas intuitively. The limit of df_{ss}/dC_s when C_g approach infinity will be

$$\lim_{C_g\to\infty}\frac{df_{ss}}{dC_s} = \frac{-1}{4\pi}\sqrt{\frac{1}{L_1}}\left(C_0+C_s\right)^{\frac{-3}{2}} = \frac{df_{\text{pp}}}{dC_s}. \tag{16}$$

Therefore,

$$\text{abs}\left(\frac{df_{ss}}{dC_s}\right) < \text{abs}\left(\frac{df_{\text{pp}}}{dC_s}\right). \tag{17}$$

It can be seen from (15) to (17) that the parallel resonance frequency of the Coil-IDE parallel topology circuit (f_{pp}) has the maximum sensitivity to the sensing capacitance (C_s).

C. Regulatory Effects of Electronic Parameters on the Sensitivity of the Parallel Resonance Frequency of Coil-IDE in Parallel Topological Structure

In the previous part, it can be noted that f_{pp} has the highest sensitivity. Next, the regulatory effects of electronic parameters on the sensitivity of f_{pp} will be analyzed.

First, the influence of the inductance value of the coil will be analyzed. Formula (10) shows that the smaller the inductance, the higher the sensitivity. For the same capacitance variation, the relationship between the frequency variation of inductance L_{11} and inductance L_{12} is $K_{12} = \sqrt{L_{12}/L_{11}}$.

Second, the influence of the capacitance value of IDE sensor will be analyzed. Formula (10) shows that the smaller the capacitance, the higher the sensitivity. For the same capacitance variation, the relationship between the frequency variation of capacitance C_{s1} and inductance C_{s2} is $K_{22} = \sqrt{(C_{s2}+C_0)/(C_{s1}+C_0)}$. Considering that $C_0 \ll C_{s2}$, $C_0 \ll C_{s1}$. It will be $K_{22} \approx \sqrt{C_{s2}/C_{s1}}$.

After the above analysis, in Section III, an experiment with the Coil-IDE humidity sensor will be applied to verify the presented results.

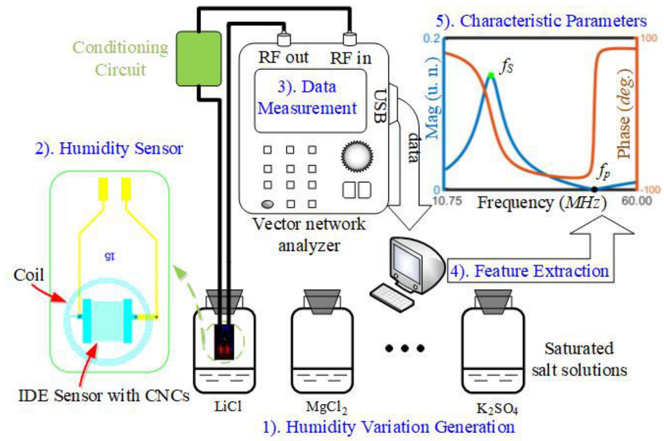

Fig. 4. Schematic of the experimental platform.

III. Experimental Platform and Sensors

In this experiment, we would like to first verify the influence of the Coil-IDE topological structure on frequency sensitivity. Then, the regulatory effect of inductance parameters and capacitance parameters on the frequency sensitivity of the sensor will be discussed. Finally, the performance of the sensor, including sensitivity, humidity reciprocation, time repeatability, and response/recovery time, will be tested.

A. Experimental Platform

The schematic of the experimental platform is shown in Fig. 4. It contains five parts: humidity variation generation, humidity sensor, data measurement, data feature extraction, and characteristic parameters.

1) Humidity Variation Generation: The humidity variation is generated by the saturated solution [7], [16]. The saturated solutions are K_2SO_4, KCl, NaCl, NaBr, $MgCl_2$, and LiCl, respectively. The fixed humidity points produced by the saturated solutions are 97.3%, 84.3%, 75.3%, 57.6%, 32.8%, and 11.3% at 25°, respectively. The experiment was carried out at room temperature (about 25°).

2) Humidity Sensor: Humidity sensing is realized by the effect of humidity on the capacitance of IDE. Resonance can improve the sensitivity and signal-to-noise ratio of the sensor information extraction. Therefore, *LC* resonance is used to extract the variation of the IDE sensor in this article. It includes two topologies: Coil-IDE in series and Coil-IDE in parallel.

3) Data Measurement: The sensor signal will be shaped by the conditioning circuit and measured by the VNA. the magnitude-frequency response of the forward transmission coefficient ($S21$) will be measured as raw data.

4) Data Feature Extraction and Characteristic Parameters: The series resonance frequency (f_s) and parallel resonance frequency (f_p) will be extracted for the magnitude-frequency curve of $S21$. The series resonance frequency (f_s) is the maximum point of the magnitude-frequency curve. The parallel resonance frequency (f_p) is the minimum one [24].

5) Characteristic Parameters Data: It contains four kinds of characteristic data: the series resonance frequency of the Coil-IDE series topology circuit (f_{ss}), the parallel resonance

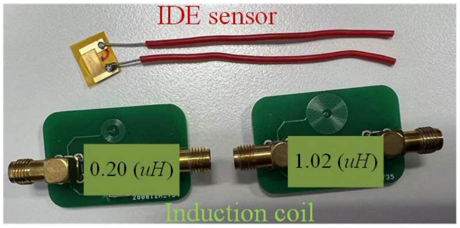

Fig. 5. PCB coil and IDE sensor.

Fig. 6. Flexible humidity sensor of Coil-IDE in parallel.

frequency of the Coil-IDE series topology circuit (f_{sp}), the series resonance frequency of the Coil-IDE parallel topology circuit (f_{ps}) and the parallel resonance frequency of the Coil-IDE parallel topology circuit (f_{pp}).

B. Sensor Fabrication

In order to compare the frequency sensitivity of series and parallel topology, we fabricated the separation devices of inductance (coil) and IDE. The humidity response of Coil-IDE with series topological structure and parallel topological structure will be measured, respectively. The printed circuit board (PCB) coil and IDE sensor are shown in Fig. 5.

In order to study the regulatory effect of inductance on the frequency sensitivity, two types of inductors are fabricated and shown at the bottom of Fig. 5. The inductances of the two inductors are 0.2 and 1.02 μH, respectively.

In order to study the regulatory effect of capacitance on the frequency sensitivity, two types of Coil-IDE sensors are fabricated and shown in Fig. 6. The IDEs of the sensors are 15 and 20 fingers respectively. The parameters of the IDE sensors are: width of the finger is 150 μm, the space between fingers is 150 μm, the length of the finger 7 mm, and the distance between the two electrodes is 130 μm.

The space and length of lead wire will caused distributed capacitance [19]. Considering that the lead spacing is difficult to maintain high-precision consistency in separate devices, we integrate coil and IDE together and adopt the same coil parameters and lead parameters. In addition, the parameters of the coils are: the radius is 10 mm, the number of turns is 3.5, and the wire diameter is 0.2 mm.

C. Sensitive Material of Humidity

In this article, cellulose nanocrystals (CNCs) and polyvinyl alcohol (PVA) are used as the humidity-sensing materials [31].

The PVA liquid was purchased in Deli Group Company Ltd., China. The CNCs powder was prepared by sulfuric acid acidified microcrystalline cellulose (MCC) according to our previous report [31]. Dispersed 90 mg of CNCs powder in 30 mL of deionized water by magnetic stirring for 30 min, and then sonicated for 2 h to form a stable CNCs suspension with a concentration of 3 mg/mL. First, it deposits a layer of PVA on the surface of IDE and lets it to dry naturally for 6 h. Second, it deposits 10 mL CNC on the surface of the PVA and dries it naturally overnight to form the humidity-sensitive film. All materials were used directly without any further processing.

IV. Results

In this section, the four frequencies of the Coil-IDE series structure [in Fig. 3(a)] and parallel structure [in Fig. 3(b)] will be compared, and the sensitivity of the four frequencies will be discussed.

A. Frequency Sensitivity Comparison of Coil-IDE Series and Parallel Topology Structure

In this experiment, the coil is a PCB coil with 1.02 μH shown in Fig. 5. The IDE sensor is also shown in Fig. 5.

First, the f_{ss} and f_{sp} of the Coil-IDE series structure were measured. The Mag of $S21$ as a function of humidity in the Coil-IDE series topological structure is shown in Fig. 7(a). As can be seen from the Fig. 7(a), f_{ss} varies with humidity, while f_{sp} has less variation. The data of f_{ss} and f_{sp} is shown in Table I.

Second, the f_{ps} and f_{pp} of the Coil-IDE parallel structure were measured. The Mag of $S21$ as a function of humidity in Coil-IDE parallel topological structure is shown in Fig. 7(b). The data of f_{ss} and f_{sp} is shown in Table I.

Third, the data in the Table I is converted into frequency variation and visualized. The frequency shift trimmed by humidity levels for the four frequencies are shown in Fig. 7(c).

In Fig. 7(c), the frequency shift of f_{sp} shows a straight line, and the variation of f_{sp} in Table I is less than 0.12 MHz. This is consistent with the (12), which predicts that the sensitivity of f_{sp} approaches 0.

The maximum frequency shifts of the other three frequencies are $\Delta f_{ss} = 4.97$ MHz, $\Delta f_{ps} = 0.75$ MHz and $\Delta f_{pp} = 10.87$ MHz. Δf_{pp} is about 14.49 times of Δf_{ps}. The frequency sensitivity of f_{pp} is greater than that of f_{ps}, which is in line with the expectation of (15).

Δf_{pp} is about 2.19 times of Δf_{ss}. The frequency sensitivity of f_{pp} is higher than that of f_{ss}, which is consistent with the (17).

Therefore, it can be found that the parallel resonance frequency of the Coil-IDE parallel topological structure has the maximum frequency sensitivity because this frequency is only regulated by the sensor capacitance.

B. Humidity Hysteresis and Response/Recovery Time

The humidity hysteresis effect is also tested in this article, where the humidity hysteresis effect is the repeatability capability of the sensor to humidity reciprocation. Chen et al. [22] mentioned that humidity hysteresis is defined as the ratio of the maximum difference between the adsorption

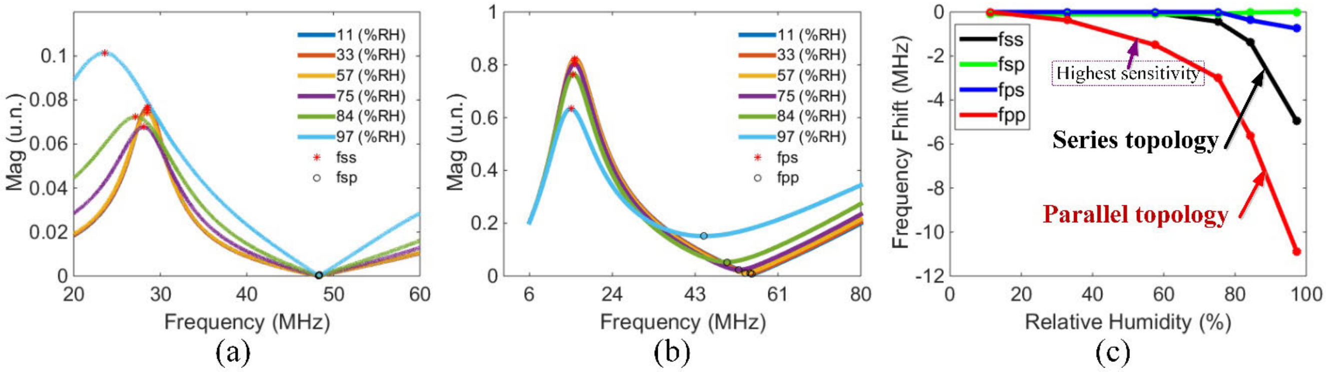

Fig. 7. Regulatory effect of humidity on frequency sensitivity in Coil-IDE series and parallel topological structure. The Mag of $S21$ as a function of humidity in Coil-IDE (a) series topological structure and (b) parallel topological structures. (c) Frequency shift regulated by humidity levels.

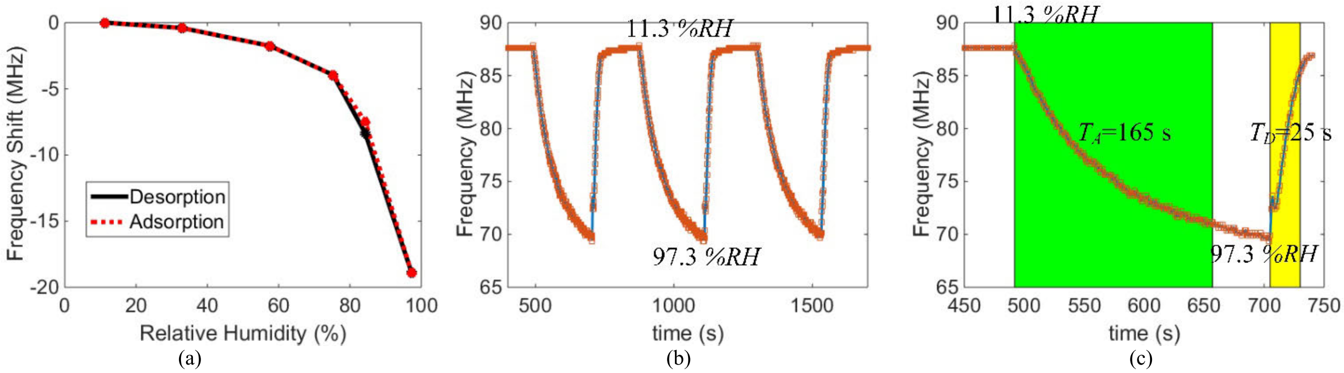

Fig. 8. Humidity hysteresis and response/recovery time. (a) Humidity hysteresis effect. (b) Response/recovery time. (c) Response/recovery time in detail.

and desorption response curves to the full response of the sensor. In this paper, the flexible sensor with 15 fingers IDE, as shown in Fig. 4 is selected to test the humidity hysteresis effect. The humidity hysteresis curves are shown in Fig. 8(a). The sensor is the flexible humidity sensor of Coil-IDE in parallel in Fig. 6. And the IDE is 15 fingers. The order in which the sensors are placed is: adsorption: K_2SO_4 $\rightarrow$KCl$\rightarrow$NaCl$\rightarrow$NaBr$\rightarrow$$MgCl_2$ $\rightarrow$LiCl; desorption: $\rightarrow$$MgCl_2$ $\rightarrow$NaBr$\rightarrow$NaCl$\rightarrow$KCl$\rightarrow$$K_2SO_4$. The maximum difference between the adsorption and desorption is 0.88 MHz at 84.30%RH, and according to the humidity hysteresis, it is 1.09%RH, which is smaller than that of most previous works [22].

The main limitation of the proposed sensor is the poor response/recovery time. The response/recovery time is defined as the time required humidity sensor to achieve 90% of the total frequency shift. The time response of the proposed Coil-IDE sensor is shown in Fig. 8(b). Fig. 8(c) is the detail of Fig. 8(b). It can be seen from Fig. 8(c) that the response/recovery time of the sensor is 165/25 s. Compared with [17], this response/recovery time is poor and may be caused by the different adsorption rates of humidity-sensitive materials [32].

V. Discussion

In the above section, experiments show that the parallel resonance frequency of the Coil-IDE parallel topological structure (f_{pp}), rather than the series resonance frequency of the Coil-IDE series topological structure (f_{ss}), has the maximum frequency sensitivity. Considering that the f_{ss} is often adopted as characterization frequency in practice by colleagues, it is necessary to study the reason why f_{pp} has higher sensitivity.

The topological circuit analysis in Section II indicates that the inevitable distributed capacitance changed the topological circuit of LC resonator, and the expression of the resonance frequency has been changed. The series resonance frequency is not only trimmed by the sensing capacitance but also by the distributed capacitance. On the contrary, another characteristic frequency, the parallel resonance frequency, is only trimmed by the sensing capacitance. Therefore, the parallel resonance frequency has higher frequency sensitivity.

In this section, we will discuss whether the experiments conform to the above theoretical expectation. First, the regulatory effect of lead capacitance on the parallel resonance frequency and series resonance frequency will be discussed. Therefore, whether the distributed capacitance changes the circuit topology and frequency expression will be verified. Second, the regulatory effect of parameters (including C_1 and L_1) on the parallel resonance frequency of the Coil-IDE parallel topological structure (f_{pp}) has been discussed, in order to facilitate the possibility of predict the sensitivity through (10). Therefore, our opinion that the parallel resonance frequency rather than the series resonance frequency is only

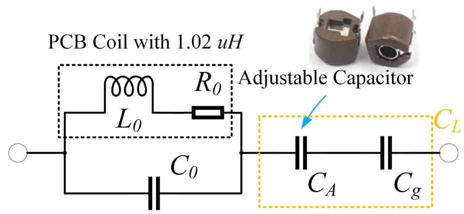

Fig. 9. Physical diagram of the circuit in the experiment of the regulatory effect of C_L on frequencies.

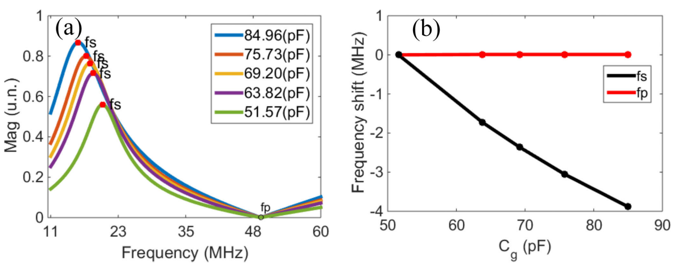

Fig. 10. Regulatory effect of C_L on frequencies. (a) Mag of $S21$ as a function of an adjustable capacitor. (b) Frequency shift as a function of an adjustable capacitor.

TABLE I
REGULATORY EFFECT OF HUMIDITY ON FREQUENCY SENSITIVITY IN COIL-IDESERIES AND PARALLEL TOPOLOGICAL STRUCTURE

Relative Humidity (% RH)	f_{ss} *(MHz)*	f_{sp} *(MHz)*	f_{ps} *(MHz)*	f_{pp} *(MHz)*
11.3	28.53	48.28	15.87	55.62
32.8	28.51	48.26	15.87	55.25
57.6	28.48	48.27	15.87	54.12
75.3	28.08	48.29	15.87	52.62
84.3	27.15	48.35	15.50	50.00
97.3	23.56	48.38	15.12	44.75

TABLE II
REGULATORY EFFECT OF C_L ON FREQUENCIES

C_L *(pF)*	f_s *(MHZ)*	f_p *(MHz)*
51.57	20.07	48.99
63.82	18.34	49.00
69.20	17.71	49.00
75.73	17.02	49.00
84.96	16.19	49.00

trimmed by the sensing capacitance will be further verified. Finally, the humidity sensitivity of the sensor in this article will be summarized.

A. Regulatory Effect of Series Capacitance on the Parallel Resonance Frequency and Series Resonance Frequency

It is generally agreed in the field of a piezoelectric crystal that the series resonance frequency can be described as $1/2\pi\sqrt{LC}$. Our research, however, found that this viewpoint is not suitable for the electronic topology of the Coil-IDE resonant circuit. As described in (5), the series resonance frequency is regulated not only by the parallel capacitance C_o but also by the series capacitance C_g.

Furthermore, it is the parallel resonance frequency only regulated by the parallel capacitance C_o and can be described as $1/2\pi\sqrt{L_1C_0}$. Therefore, a circuit with structure as in Fig. 1 is designed to support the proposed viewpoint.

The physical diagram of the circuit in the experiment is shown in Fig. 9. In this circuit, C_L is the value of adjustable inductance and grounding capacitance in series, the L_1 is the PCB coil with the inductance value of 1.02 μH, the C_0 is a chip capacitor with a capacitance of 10 pF.

The response of amplitude-frequency-curves to adjustable capacitor is shown in Fig. 10(a), and the frequency shift of series resonance frequency (f_s) and parallel resonance frequency (f_p) to the variation of adjustable capacitor is shown in Fig. 10(b). It can be found that adjustable capacitor (series capacitance) has an obvious regulatory effect on f_s, and less regulatory effect on f_p.

Those data are given in Table II. The C_L, f_s, and f_p is measured by the method in reference [19] based on the VNA. The standard deviation (STD) of f_s is 146.90%, and the STDs of f_p is 0.45%. Those STDs indicate that the parallel resonance frequency (f_p) only regulated by the parallel capacitance C_0 and not regulated by the series capacitance C_g. Therefore, it can be conclusion that, for Coil-IDE resonant circuit, it is the parallel resonance frequency (f_p) can be described as $1/2\pi\sqrt{L_1C_0}$ and not the series resonance frequency (f_s).

Considering that the parallel resonance frequency is regulated by lesser capacitance, if the IDE capacitance sensor is parallel with the coil, the sensing capacitance will have higher frequency sensitivity to sensing capacitance variation, although this viewpoint is opposite to the field of quartz crystal.

B. Regulatory Effect of L_1 on the Frequency Sensitivity

In order to study the regulatory effect of the inductance value L_1 on the variation of parallel frequency of Coil-IDE parallel structure (f_{pp}), two kinds of inductance value coils (1.02 and 0.2 μH) was fabricated. The inductance value is measured by the method in [19]. The two inductances that connect the same IDE, respectively. Their response of amplitude-frequency curves to humidity are shown in Fig. 11(a) and (b) respectively.

The frequency shift trimmed by humidity levels under different inductances is shown in Fig. 11(c). In addition, the data of f_{pp} in Fig. 11(a) and (b) are shown in Table III.

In Table III, the K_{11} is defined as

$$K_{11} = \frac{f_{\mathrm{pp}}\big|_{L_1=1.02,\mathrm{humidity}=H_i}}{f_{\mathrm{pp}}\big|_{L_1=0.2,\mathrm{humidity}=H_i}} \tag{18}$$

where, $f_{\mathrm{pp}}\big|_{L_1=x,\mathrm{humidity}=H_i}$ is the frequency shift generated by the same humidity H_i, when the capacitance of the IDE sensors is x.

At the max humidity of 97.3%, the f_{pp} are $f_{\mathrm{pp}}\big|_{L_1=1.02,\mathrm{humidity}=97.3\%} = 44.75$ (MHz) and $f_{\mathrm{pp}}\big|_{L_1=0.2,\mathrm{humidity}=97.3\%} = 85.47$ (MHz), respectively. In this moment, the K_{11} is 0.52.

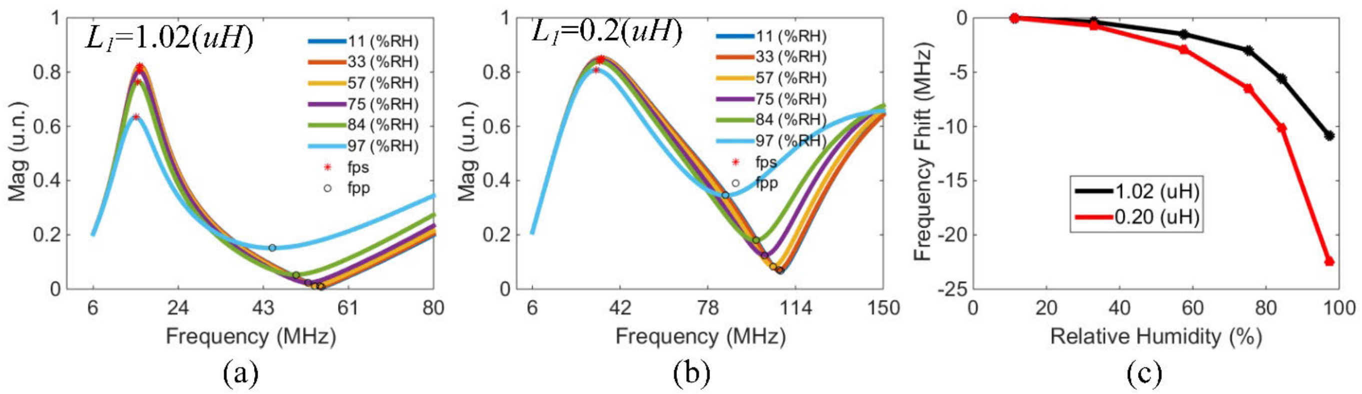

Fig. 11. Regulatory effect of coil inductance on frequency sensitivity in Coil-IDE parallel topological structure. The Mag of $S21$ as a function of humidity when the coil inductance is (a) 1.02 and (b) 0.2 μH. (c) Frequency shift trimmed by humidity levels under different coil inductance.

TABLE III
REGULATORY EFFECT OF COIL INDUCTANCE ON FREQUENCY SENSITIVITY INCOIL-IDE PARALLEL TOPOLOGICAL STRUCTURE

Relative Humidity (% RH)	f_{pp} (MHz)		K_{11}	Error relative to formula (10) prediction
	L_1= 1.02(uH)	L_1= 0.2(uH)		
11.3	55.62	107.95	0.52	14.06%
32.8	55.25	107.22	0.52	14.07%
57.6	54.12	105.05	0.52	14.05%
75.3	52.63	101.43	0.52	14.66%
84.3	50.00	97.80	0.51	13.39%
97.3	44.75	85.47	0.52	15.43%

TABLE IV
REGULATORY EFFECT OF IDE CAPACITANCE ON FREQUENCY SENSITIVITY INCOIL-IDE PARALLEL TOPOLOGICAL STRUCTURE

Relative Humidity (% RH)	f_{pp} (MHz)		K_{21}	Error relative to formula (10) prediction
	15 fingers	20 fingers		
11.3	88.60	80.24	0.91	9.16%
32.8	88.12	80.01	0.91	8.88 %
57.6	87.17	79.36	0.91	8.59%
75.3	84.80	77.16	0.91	8.65%
84.3	81.00	74.08	0.91	8.09%
97.3	69.12	63.52	0.92	7.57%

It can be predicted from (10) that the value of K_{11} should be the square root of the ratio of the two inductances under arbitrary humidity. Therefore, the predicted value of K_{11} would be $K_{12} = \sqrt{0.2/0.02} = 0.44$.

Compared with the data of K_{11} in Table III, the error between K_{11} and K_{12} is about 13.39% to 15.43%. The low error between K_{11} and K_{12} shows a qualitative significance of (10) to predict the frequency sensitivity regulated by the parallel inductance.

C. Regulatory Effect of C_1 on the Frequency Sensitivity

In order to study the regulatory effect of the capacitance value C_1 on $f_{\rm pp}$, two kinds (15 and 20 fingers) of capacitance value IDE sensors were fabricated. The IDE sensors are parallel with the coil, which has the same geometric parameters. The capacitance value of the two IDE is measured by the method in [19]. The measured capacitance values of IDE without sensitive materials add the windings capacitance of the coil are 0.63 and 0.80 pF, respectively.

The response of amplitude-frequency-curves to humidity are shown in Fig. 12(a) and (b), respectively. The frequency shift trimmed by humidity levels under different IDE sensors is shown in Fig. 12(c). In addition, the data of $f_{\rm pp}$ in Fig. 12(a) and (b) are shown in Table IV.

In Table IV, the K_{21} is defined as

$$K_{21} = \frac{f_{\rm pp}\big|_{C_1=0.80,\text{humidity}=H_i}}{f_{\rm pp}\big|_{C_1=0.63,\text{humidity}=H_i}} \tag{19}$$

where, $f_{\rm pp}\big|_{C_1=x,\text{humidity}=H_i}$ is the frequency generated by the same humidity H_i, when the capacitance of the IDE sensors is x.

At the max humidity of 97.3%, the $f_{\rm pp}$ are $f_{\rm pp}\big|_{C_1=0.80,\text{humidity}=97.3\%} = 63.53$ (MHz) and $f_{\rm pp}\big|_{C_1=0.80,\text{humidity}=97.3\%} = 69.12$ (MHz), respectively. In this moment, the K_{21} is 0.92.

It can be predicted from (10) that the value of K_{21} should be the square root of the ratio of 0.63 and 0.80 pF. Therefore, the predicted value of K_{21} should be $K_{22} \approx \sqrt{0.63/0.88} = 0.89$. If the capacitance ratio is replaced by the ratio of the fingers of the IDE, then the predicted value will be $K'_{22} \approx \sqrt{15/20} = 0.87$.

Compared with the data of K_{21} in Table IV, the error between K_{21} and K_{22} is about 7.57%–9.16%. The low error between K_{21} and K_{22} shows a qualitative significance of (10) to predict the frequency sensitivity regulated by the capacitance value of the IDE sensor.

D. Frequency Sensitivity Comparison

High humidity sensitivity is achieved in this article. The achieved sensitivity is shown in Table V. The flexible Coil-IDE with 15 fingers has the highest humidity sensor. It is 2556.43 ppm/%RH (0.23 MHz/%RH) with a range of 11%–97% and working frequency of 88.60 MHz. This result is reached the performance of [1].

Further more, eliminating low humidity points, the proposed Coil-IDE humidity sensor obtained a sensitivity

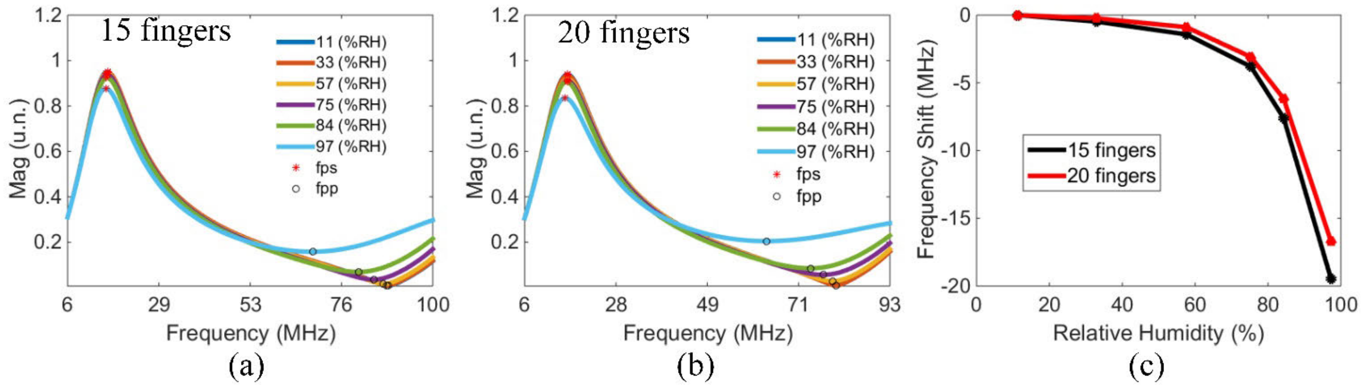

Fig. 12. Regulatory effect of IDE capacitance on frequency sensitivity in Coil-IDE parallel topological structure. The Mag of $S21$ as a function of humidity when the IDE is (a) 15 and (b) 20 fingers. (c) Frequency shift trimmed by humidity levels under different IDE capacitance.

TABLE V
ACHIEVED SENSITIVITY

Type	*Sensitivity*		*RH Range (%)*	*Operating frequency (MHz)*
	MHz/%RH	*ppm/%RH*		
0.20 *uH* PCB	0.26	2421.44	11-97	107.95
1.02 *uH* PCB	0.13	2272.48	11-97	55.62
15 fingers flexible	0.23	2556.43	11-97	88.60
15 fingers flexible	0.29	3342.86	32-97	88.60
20 fingers flexible	0.19	2430.23	11-97	80.24

of 3342.86 ppm/%RH (0.29 MHz/%RH) with a range of 32%–97% and working frequency of 88.60 MHz.

VI. Conclusion and Future Work

In this article, the frequency sensitivity of the Coil-IDE resonant topology circuit has been analyzed through the proposed inverse transformation of the equivalent conversion between Coil-IDE resonant topological circuits and the piezoelectric crystal topology circuit. First, the formula of the resonance frequencies under different integrated topologies of Coil and IDE is proposed. Second, the sensitivity of the resonance frequencies of the Coil-IDE integrated sensor under different topological structures is compared mathematically. Then, the frequency sensitivity is compared by a humidity-sensing application of the Coil-IDE sensor through different integrated topologies and parameters. Finally, the following conclusions can be drawn.

1) The inverse transformation of the equivalent conversion between the Coil-IDE resonant sensor topology circuit and the piezoelectric crystal topology circuit is proposed in (4). Through this inverse transformation, four frequency expressions representing the Coil-IDE topology structure in series and parallel are proposed, respectively. The coil winding capacitance and grounding capacitance has been considered in those formulas, which is more conducive to high-frequency applications.
2) The sensitivity of four frequencies to IDE capacitance variation was analyzed. It is found that parallel resonance frequency of Coil-IDE parallel topological circuit (f_{pp}) has the highest frequency sensitivity. Coil-IDE humidity sensor experiments show that the frequency shift of f_{pp} trimmed by humidity variation is 2.19 times higher than that of the series resonance frequency of the Coil-IDE series topological circuit (f_{ss}).
3) The regulatory effects of inductance and capacitance parameters on the sensitivity of f_{pp} to IDE capacitance variation is in line with the expectation of the proposed (10) in high humidity. The ratio of frequency shifts of f_{pp} using 1.02 and 0.2 μH inductance is about 0.48, which is close to the square root of inductance ratio (0.44); The ratio of frequency shifts of f_{pp} using 0.63 and 0.80 pF capacitance (corresponding to 15 and 20 interdigital IDE) is about 0.86, which is close to the square root of capacitance ratio 0.89. The error is as low as 7.57% in high humidity.
4) Based on the proposed regulation mechanism of topology circuit and parameters on sensitivity, a higher sensitivity was obtained. The proposed Coil-IDE humidity sensor shows a high sensitivity of 0.29 MHz/%RH, 3342.86 ppm/%RH in the humidity range of 32%–97%.
5) The main limitation of the proposed sensor is the poor response/recovery times. The response/recovery times of the sensors is as long as 165/25 s.

Future work will focus on the miniaturization of the signal processing system and its application in distributed monitoring of indoor humidity in civil buildings and smart homes.

References

[1] Y. Feng, L. Xie, Q. Chen, and L.-R. Zheng, "Low-cost printed chipless RFID humidity sensor tag for intelligent packaging," *IEEE Sensors J.*, vol. 15, no. 6, pp. 3201–3208, Jun. 2014.

[2] L. Dong, L.-F. Wang, and Q.-A. Huang, "A passive wireless adaptive repeater for enhancing the readout of LC passive wireless sensors," *IEEE Microw. Wireless Compon. Lett.*, vol. 26, no. 7, pp. 543–545, Jul. 2016.

[3] M. A. Martuza, C.-H. Lee, A. Sazonov, S. Boumaiza, and K. S. Karim, "Wireless LC-type passive humidity sensor using large-area RF magnetron sputtered ZnO films," *IEEE Trans. Electron Devices*, vol. 65, no. 8, pp. 3447–3453, Aug. 2018.

[4] W.-J. Deng, L.-F. Wang, L. Dong, and Q.-A. Huang, "Experimental study of the bending effect on LC wireless humidity sensors fabricated on flexible PET substrates," *J. Microelectromech. Syst.*, vol. 27, no. 5, pp. 761–763, Oct. 2018.

[5] M.-Z. Xie, L.-F. Wang, B.-B. Zhou, and Q.-A. Huang, "An impedance matching method for LC passive wireless sensors," *IEEE Sensors J.*, vol. 20, no. 22, pp. 13833–13841, Nov. 2020.

[6] S. Su, W. Lv, T. Zhang, Q. Tan, W. Zhang, and J. Xiong, "A MoS_2 nanoflakes-based LC wireless passive humidity sensor," *Sensors*, vol. 18, no. 12, p. 4466, Dec. 2018.

[7] Q. Chen, X.-H. Huang, Y. Yao, K.-B. Luo, H.-Z. Pan, and Q. Wang, "Ringed electrode configuration enhances the sensitivity of QCM humidity sensor based on lignin through fringing field effect," *IEEE Sensors J.*, vol. 21, no. 20, pp. 22450–22458, Oct. 2021.

[8] X. Ding, X.-D. Chen, X.-L. Yu, and X. Yu, "A GOQD modified IDE-PQC humidity sensor based on impedance-frequency tuning principle with enhanced sensitivity," *Sens. Actuators B, Chem.*, vol. 276, pp. 288–295, Dec. 2018.

[9] S. Alam, T. Islam, and U. Mittal, "A sensitive inexpensive SAW sensor for wide range humidity measurement," *IEEE Sensors J.*, vol. 20, no. 1, pp. 546–551, Jan. 2020.

[10] W. Lv, Q. Tan, H. Kou, W. Zhang, and J. Xiong, "MWCNTs/WS_2 nanocomposite sensor realized by LC wireless method for humidity monitoring," *Sens. Actuators A, Phys.*, vol. 290, pp. 207–214, May 2019.

[11] H. Wen et al., "Array integration and far-field detection of biocompatible wireless LC pressure sensors," *Small Methods*, vol. 5, no. 3, Mar. 2021, Art. no. 2001055.

[12] Z. Bu, L. Liu, C. Zhong, S. Wang, D. Gu, and L. Wang, "An innovative LC-C resonant pressure sensor based on capacitive feedthroughs," *IEEE Sensors J.*, vol. 21, no. 18, pp. 19825–19832, Sep. 2021.

[13] A. Biswas, S. Yin, M. Tursunniyaz, N. KaramiMohammadi, J. Huang, and J. Andrews, "Geometrical optimization of printed interdigitated electrode sensors to improve soil moisture sensitivity," *IEEE Sensors J.*, vol. 22, no. 20, pp. 19162–19169, Oct. 2022.

[14] Z. Duan, Y. Jiang, and H. Tai, "Recent advances in humidity sensors for human body related humidity detection," *J. Mater. Chem. C*, vol. 9, no. 42, pp. 14963–14980, Nov. 2021.

[15] L. Zhang, Q. Tan, H. Kou, D. Wu, W. Zhang, and J. Xiong, "Highly sensitive NH_3 wireless sensor based on Ag-RGO composite operated at room-temperature," *Sci. Rep.*, vol. 9, no. 1, p. 9942, Jul. 2019.

[16] Q. Chen, Y. Yao, X. H. Huang, D. Liu, and K. L. Mao, "Simulation analysis and experimental verification for sensitivity of IDE-QCM humidity sensors," *Sens. Actuators B, Chem.*, vol. 341, Aug. 2021, Art. no. 129992.

[17] L. Zhang et al., "Wirelessly powered multi-functional wearable humidity sensor based on RGO-WS_2 heterojunctions," *Sens. Actuators B, Chem.*, vol. 329, Feb. 2021, Art. no. 129077.

[18] A. Ebrahimi, J. Scott, and K. Ghorbani, "Ultrahigh-sensitivity microwave sensor for microfluidic complex permittivity measurement," *IEEE Trans. Microw. Theory Techn.*, vol. 67, no. 10, pp. 4269–4277, Oct. 2019.

[19] D. Liu et al., "RLC parameters measurement and fusion for high-sensitivity inductive sensors," *IEEE Trans. Instrum. Meas.*, vol. 71, pp. 1–11, 2022.

[20] D. Wu, W. Chen, J. Yang, and F. Yang, "Self-resonance eddy-current testing method in noncontact detection of carbon fiber reinforced plastics," *Compos. Struct.*, vol. 259, Mar. 2021, Art. no. 113247.

[21] L. U. Daura and G. Y. Tian, "Wireless power transfer based non-destructive evaluation of cracks in aluminum material," *IEEE Sensors J.*, vol. 19, no. 22, pp. 10529–10536, Nov. 2019.

[22] C.-M. Chen, J. Xu, and Y. Yao, "Fabrication of miniaturized CSRR-loaded HMSIW humidity sensors with high sensitivity and ultra-low humidity hysteresis," *Sens. Actuators B, Chem.*, vol. 256, pp. 1100–1106, Mar. 2018.

[23] B.-B. Zhou, W.-J. Deng, L.-F. Wang, L. Dong, and Q.-A. Huang, "Enhancing the remote distance of LC passive wireless sensors by parity-time symmetry breaking," *Phys. Rev. Appl.*, vol. 13, no. 6, Jun. 2020, Art. no. 064022.

[24] V. E. Bottom, *Introduce to Crystal Unite Design*. New York, NY, USA: Van Nostrand Rcinhold Company, 1987.

[25] J. R. Vig. *Quartz Crystal Resonators and Oscillators for Frequency Control and Timing Applications—A Tutorial*. Accessed: Jan. 2000. [Online]. Available: https://www.am1.us/wp-content/uploads/Documents/U11625_VIG-TUTORIAL.pdf

[26] B. L. Cannon, J. F. Hoburg, D. D. Stancil, and S. C. Goldstein, "Magnetic resonant coupling as a potential means for wireless power transfer to multiple small receivers," *IEEE Trans. Power Electron.*, vol. 24, no. 7, pp. 1819–1825, Jul. 2009.

[27] T. Funck, A. Müller, and H. Bothe, "Synthetic inductance standards made up of capacitances and gyrators," *IEEE Trans. Instrum. Meas.*, vol. 70, pp. 1–4, 2021.

[28] R. Hughes, Y. Fan, and S. Dixon, "Near electrical resonance signal enhancement (NERSE) in eddy-current crack detection," *NDT E Int.*, vol. 66, pp. 82–89, Sep. 2014.

[29] A. Abderahim, A. T. Mahamat, J. P. Chatelon, D. Pietroy, S. Capraro, and J. J. Rousseau, "Approach of copper losses determination in planar windings," *Electron. Lett.*, vol. 52, pp. 1050–1051, Jun. 2016.

[30] *Measurement of Quartz Crystal Unit Parameters—Part 5: Methods for the Determination of Equivalent Electrical Parameters Using Automatic Network Analyzer Techniques and Error Correction*, International Electro technical Commission, London, U.K., 1995.

[31] J. Liu, Z. Zhao, Z. Fang, Z. Liu, Y. Zhu, and L. Du, "High-performance FBAR humidity sensor based on the PI film as the multifunctional layer," *Sens. Actuators B, Chem.*, vol. 308, Apr. 2020, Art. no. 127694.

[32] Y. Lu et al., "Highly stable Pd/HNb_3O_8-based flexible humidity sensor for perdurable wireless wearable applications," *Nanosc. Horizons*, vol. 6, no. 3, pp. 260–270, Mar. 2021.

Dong Liu (Member, IEEE) received the B.Sc. degree in physics from Sichuan University, Chengdu, China, in 2004, and the M.Sc. and Ph.D. degrees in control science and engineering from the University of Electronic Science and Technology of China, Chengdu, in 2010 and 2017, respectively.

He is currently a Research Associate with the School of Automation Engineering, University of Electronic Science and Technology of China. His research interests include crystal oscillators, piezoelectric sensors, humidity sensors, and eddy current sensors.

Qiao Chen was born in Sichuan, China, in 1996. He received the B.S. degree from the North University of China, Taiyuan, China, in 2017. He is currently pursuing the Ph.D. degree with the School of Automation and Engineering, University of Electronic Science and Technology of China, Chengdu, China.

His current research interests include the mass sensitivity of quartz crystal microbalance, humidity sensors, and gas sensors.

Haoran Li received the B.Sc. degree in electrical engineering and automation and the M.Sc. degree in control science and engineering from the Southwest University of Science and Technology, Mianyang, China, in 2015 and 2018, respectively, and the Ph.D. degree in control science and engineering from the University of Electronic Science and Technology of China, Chengdu, China, in 2022.

He is currently engaged in teaching and research works with the Southwest University of Science and Technology. His research interests mainly focus on eddy current testing and thermography, instrumentation manufacturing, and power electronics technology.

Guiyun Tian (Senior Member, IEEE) received the B.Sc. degree in metrology and instrumentation and the M.Sc. degree in precision engineering from the University of Sichuan, Chengdu, China, in 1985 and 1988, respectively, and the Ph.D. degree from the University of Derby, Derby, U.K., in 1998.

From 2000 to 2006, he was a Lecturer, a Senior Lecturer, a Reader, a Professor, and the Head of the Group of Systems Engineering, University of Huddersfield, Huddersfield, U.K. Since 2007, he has been with Newcastle University, Newcastle upon Tyne, U.K., where he has been a Chair Professor in Sensor Technologies. Currently, he is an Adjunct Professor with the School of Automation Engineering, University of Electronic Science and Technology of China, Chengdu. He has coordinated several research projects from the Engineering and Physical Sciences Research Council (EPSRC), Royal Academy of Engineering, and FP7, on top of this he also has good collaboration with leading industrial companies such as Airbus, Rolls Royce, BP, nPower, Networkrail, and TWI among others, Europe.

Bin Gao (Senior Member, IEEE) received the B.Sc. degree in communications and signal processing from Southwest Jiaotong University, Chengdu, China, in 2005, and the M.Sc. (Hons.) degree in communications and signal processing and the Ph.D. degree from Newcastle University, Newcastle upon Tyne, U.K., in 2006 and 2011, respectively.

From 2011 to 2013, he worked as a Research Associate with Newcastle University, on wearable acoustic sensor technology. He is currently a Professor with the School of Automation Engineering, University of Electronic Science and Technology of China (UESTC), Chengdu. He is also a very active reviewer for many international journals and long-standing conferences. He has coordinated several research projects from the National Natural Science Foundation of China. His research interests include electromagnetic and thermography sensing, machine learning, and nondestructive testing and evaluation, and he actively publishes in these areas. More information can be found at: http://faculty.uestc.edu.cn/gaobin/zh_CN/lwcg/153392/list/index.htm.

Zhuhong Xiong received the B.Sc. degree in civil engineering from Southwest Jiaotong University, Chengdu, China, in 2004.

She is currently working as a Senior Engineer with Sichuan Institute of Building Research Company Ltd., Chengdu. She is the Director of the Innovation Research Center of Sichuan Craftsman, Chengdu. Her current research interests are mainly intelligent monitor of underground engineering water penetration, buoyant force, and deformation.

Dr. Xiong has been awarded the National May 1 Labor Medal and the Reserve Candidates for Academic and Technical Leaders in Sichuan Province.

Minqiang Li received the B.S. degree from the School of Automation, Xi'an University of Posts and Telecommunications, Xi'an, Shanxi, China, in 2003. He is currently pursuing the Ph.D. degree with the College of Materials Science and Engineering, Sichuan University, Chengdu, China.

His current research interests include the quartz crystal microbalance, piezoelectric sensor, and thin film preparation technology.